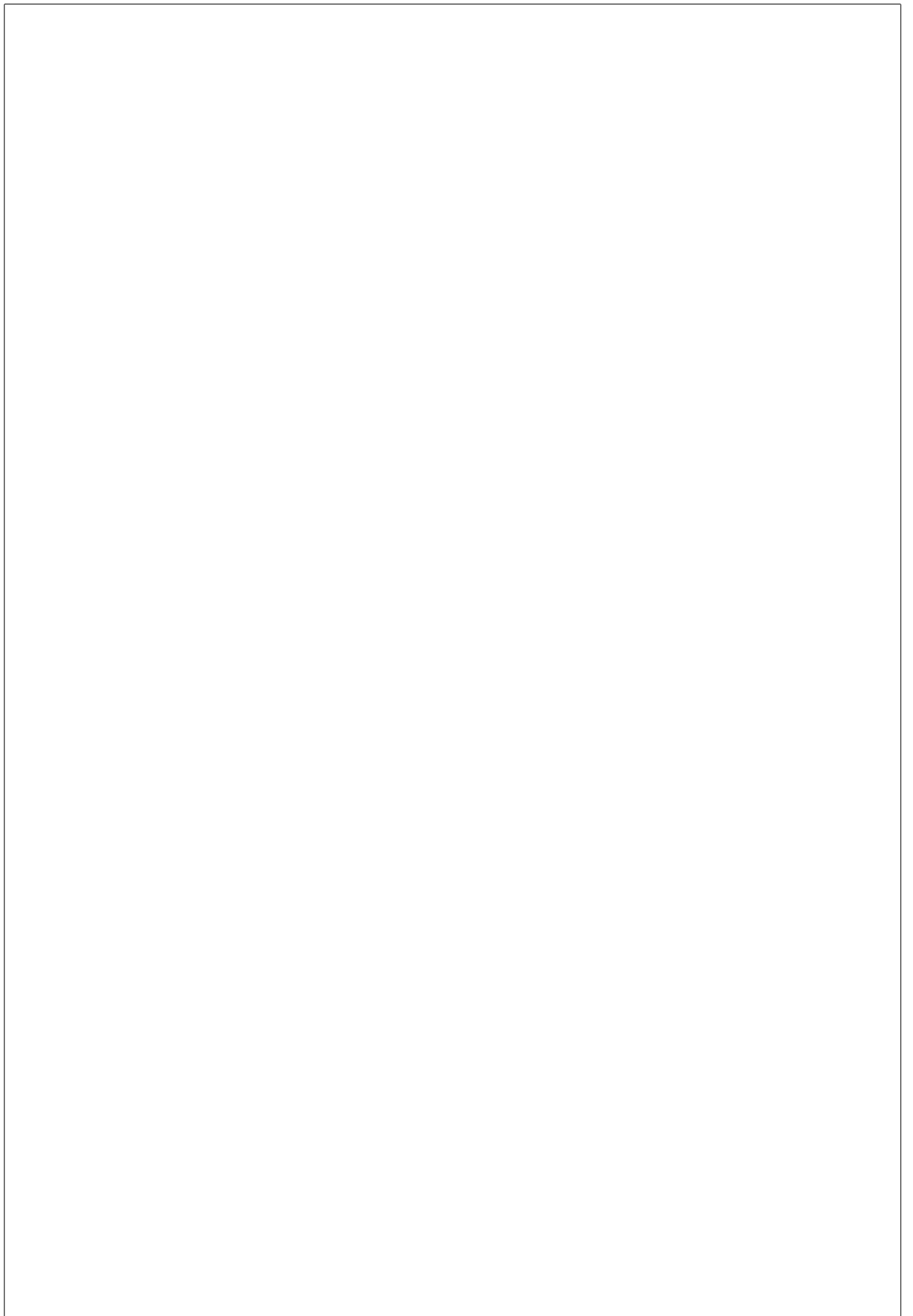


---

---



---

---

---

## **Todo list**

cps zu a.u. aendern . . . . .	20
zahlen fuer sat eintragen . . . . .	20
put in pictures for fdtd results and reference them . . . . .	21

---

---

# Contents

<b>Table of Contents</b>	<b>i</b>
<b>List of Tables</b>	<b>i</b>
<b>1 Introduction</b>	<b>1</b>
1.1 Coupling Nanodiamonds to Optical Antennas . . . . .	5
1.1.1 Plasmonic Antennas . . . . .	5
1.1.2 Plasmonic Antenna Design and Simulation . . . . .	9
1.1.3 SiV center in a Plasmonic Double Bowtie Antenna . . . . .	11
<b>Bibliography</b>	<b>23</b>

---

---

---

## List of Tables

---

---

---

# Chapter 1

## Introduction

“Every competent physicist can “do” quantum mechanics, but the stories we tell ourselves about what we are doing are as various as the tales of Sheherazade, and almost as implausible.”

David J. Griffiths

The International System of Units (SI, abbreviated from the French Système international d’unités) emerged in the late 18<sup>th</sup> century as a coherent metric system of measurement with rationally related units and simple rules for combining them [?]. Since its inception it was improved and augmented continuously in an ongoing effort to accommodate continued scientific and technological progress. The current SI system is comprised of seven base units: The kilogram (kg), the second (s), the Ampere (A), the Kelvin (K), the mole (mol) and the candela (cd). Currently a redefinition of four of base units (kilogram, mole, Kelvin, Ampere) in terms of fundamental constants is under way [?, ?, ?]. The proposed change will improve the definitions of these base units to make them easier to realize experimentally, particularly for the measurement of electrical quantities [?]. It will also eliminate the last remaining base unit definition which relies on a historic material artifact, the international prototype of the kilogram. As a result all base units will, for the first time, be tied to one or more fundamental constants of nature.

As these developments are put into motion, similar discussions regarding the SI base unit for luminous intensity, the candela, have emerged. It has been suggested that it can be improved by leveraging recent advances in classical radiometry and photometry as well as the development of novel quantum devices and techniques [1].

At the time of writing the definition of the candela read:

The candela is the luminous intensity, in a given direction, of a source that emits monochromatic radiation of frequency  $540 \times 10^{12}$  Hz and that has a radiant intensity in that direction of  $638^{-1} \text{W sr}^{-1}$ .

Traditional applications relying on this definition in conjunction with accurate photometric and radiometric measurements are light design, manufacturing and use of optical

sources, detectors, optical components, colored materials and optical radiation measuring equipment [?]. In the classical regime of optical radiation high flux levels dominate. Here primary optical radiation scales for sources and detectors are generally based on cryogenic radiometry establishing a link to the SI units of electricity [?]. Other calculable sources such as synchrotron and blackbody radiators can serve as primary source scales in the ultraviolet and deep-UV regions by establishing traceability to SI units of thermometry, electricity and length [?, 1].

Scaling down to the quantum world of radiometry is associated with a loss of measurement accuracy. In this regime dedicated photon counting techniques are required to deal with the challenge of low flux levels. Since they rely on counting photons directly, in principle they can provide efficient and traceable measurements and improved uncertainties. For high-accuracy absolute radiometry in this regime, predictable single or quasi-single-photon sources and photon detectors as well as associated new quantum-based calibration methods and standards are called for. To promote the development of such technologies a reformulation of the candela has been proposed in terms of *countable* photon units [?, 1, ?, ?, ?]. Here we emphasize the distinction between *countable* and *calculable* sources of photons. The latter being available as blackbodies or synchrotron radiators.

A straightforward quantum-based reformulation has been suggested based on [1, ?]:

$$P = nh\nu, \quad (1.1)$$

where the radiant intensity per steradian  $P = 638^{-1}\text{W sr}^{-1}$  in a given direction and the photon frequency  $\nu = 540 \times 10^{12}\text{ Hz}$  are assumed to be exact with their numerical values inherited from the present definition of the candela. The anticipated proposed changes to the SI system will define Planck's constant  $h = 6.626\,070\,15 \times 10^{-34}\text{ J s}$  as an exact numerical constant [?]. As a consequence the number of photons per second per steradian in a candela  $n$  becomes a constant defined as:

$$n = \frac{P}{h\nu} \approx 4.091\,942\,9 \times 10^{15} \text{ counts s}^{-1} \text{ sr}^{-1}. \quad (1.2)$$

Given this definition of the radiant intensity of a candela in terms of countable photons, a possible formulation of the quantum candela could read:

The candela is the luminous intensity, in a given direction, of a source that emits photons of frequency  $540 \times 10^{12}\text{ Hz}$  at a rate of  $4.091\,942\,9 \times 10^{15}$  photons per second per steradian in that direction.

This definition would incur a deviation of 0.0014 % from the current value of the candela. This is an acceptable change, taking into account the fact that current experimental realizations of the candela are limited to uncertainties of 0.02 % [1]. Proposals such as this are regularly reviewed by the Consultative Committee for Photometry and Radiometry ensuring that the current best measurement practices and existing as well as emerging needs of the user community of the candela are met [?].

While a proposed formulation of a quantum-candela can be considered a small change to the SI system, a shift towards quantum based radiometric SI units is likely to become a critical enabler driving the development of accurate and traceable measurement methods on the single-photon level. In order for the definition of the quantum-candela to have practical meaning, photon counting detectors are required capable of accurately resolving single-photons. To ensure proper calibration of such devices, reliable deterministic single photon sources are key. As novel instruments and associated calibration standards emerge, our ability to work with individual photons in a wide range of applications is expected to improve [?, ?, ?, ?]. The quest for single photon sources is supported by large research projects such as "Single-Photon Sources for Quantum Technology" funded by European Metrology Research Program.

Advances in radiometry are particularly important for fields like quantum communication and quantum computing. They are heavily reliant on deterministic reliable single-photon sources and well-calibrated detectors. As such they have proven to be major driving forces in their development [?, ?]. Amongst others, some well known applications include quantum key distribution [?, ?, ?] or transmission in a quantum network [?, ?, ?].

At present several candidates for on-demand single-photon sources are available, which we shortly mention here. One possibility consists of using a laser beam attenuated such that the mean number of photons in the beam becomes close to one [?, ?, ?]. However, the mean photon number cannot be controlled perfectly and a non-zero probability remains that multiple photons are present in the beam simultaneously.

Quasi-single photon states can be realized more efficiently using photon-pairs consisting of a signal and an idler photon. Pairs are created when a photon interacts with a non-linear optical medium in a process called spontaneous parametric down-conversion (SPDC) [?, ?, ?, ?, ?, ?]. The deciding feature of the process is the strong time-correlation between signal and idler photons. If both photons are injected into individual signal paths, an detection event in one of the paths heralds the existence of a photon in the other path. SPDC pairs can thus be used to construct single-photon sources. Unfortunately, due to the poor efficiency of the SPDC process, the probability of generating pairs is unfavorable [?, 2]. Thus efforts have been undertaken to improve the efficiency [2, ?, ?].

Quantum dots emit photons by recombination of electron-hole pairs created by optical excitation or via an electric current [?, ?, ?]. The choice of semi-conducting material determines the electronic structure of the system and thus the characteristics of the emitter. Similarly, single-photons can be obtained as a result of radiative transitions between energy levels of single atoms or molecules trapped in an optical cavity [?]. While these sources have desirable properties such as high-collection efficiency, the practical usefulness is limited due to being technologically demanding. Amongst others a high vacuum is needed to operate these sources [?].

For a wide range of single photon sources, significant progress has been made towards improving purity, indistinguishability and collection efficiency [?, ?, ?, ?, ?].

As it stands, a single photon source suitable for the calibration of single-photon detectors remains difficult to realize [?]. Ideally, a standard single photon source should be emitting with a quantum efficiency of 100 % indicating that the entire excitation energy is transformed into radiation without losses. At the same time single photons should be emitted with a probability of one and subsequently collected with perfect efficiency.

Very recently, another interesting direction has been explored, identifying color centers in nanodiamonds involving silicon [?, ?] and nitrogen [?] as promising candidates for the realization of standard single photon sources [3, 4]. In particular it was shown that it is possible to absolutely calibrate single photon sources using a classical detector and a calibrated spectrometer, establishing an unbroken traceability chain to the SI system. The photon flux of the source can be controlled via the settings of the pump laser repetition rate. In this way a direct link between the high photon flux levels of the classical regime and low photon flux levels in the quantum world has been formed. For the nitrogen vacancy center a photon flux rate of  $\approx 1.4 \times 10^5$  photons per second was recorded.

In this thesis we continue researching the potential of color centers in diamond as single photon sources. More precisely, we focus on the silicon-vacancy center. In doing so we aim to add momentum to the development of single photon source as high-accuracy calibration devices and subsequently, to the development of photon counting detectors and the adoption of the quantum-candela.

The SiV center in diamond is an ideal candidate for single photon calibration purposes. It is a very efficient and stable narrow linewidth emitter, producing single photons with high intensity. Conveniently, SiV centers operate at room temperature under normal pressure and hence do not require overly sophisticated experimental setups. As an alternative to hosting SiV centers in bulk diamond, they can be implanted in nano-sized diamond grains offering increased collection efficiency. Grains containing individual SiV centers can be identified and preselected according to their properties.

In this thesis we synthesize nanodiamonds with SiV centers using a variety of different techniques. Chemical vapor deposition, high-pressure, high-temperature synthesis as well as wet-milling methods are used to produce a sizable set of samples. To investigate the samples, i.e. to study the optical properties of embedded SiV centers we rely on optical excitation. In particular, confocal microscopy is used to collect emitted fluorescent single-photons. An attached spectrometer or a Hanbury Brown and Twiss setup offer further insights into the properties of the SiV center as a single photon source.

Our work can roughly be subdivided into two larger explorations. The first revolves around charting the luminescence properties of a large set of nanodiamonds and their hosted emitters, allowing us to establish distributions of selected SiV center properties. To our knowledge, our efforts result in the largest coherent examination of SiV centers in nanodiamonds to date. In contrast to that the second exploration focuses on individual nanodiamonds and our attempts to relocate them to different nano structures in order to achieve a coupling between SiV centers and the host structure. First we attempt to realize a controllable hybrid-integrated single photon source by placing a

nanodiamond containing SiV centers on top of a vertical-cavity surface emitting laser (VCSEL). Furthermore, we combine nanodiamonds with plasmonic nano-antennas in order to enhance the emission properties of the contained SiV centers. To this aim, a range of samples were investigated in the search for well-suited nanodiamonds hosting single SiV centers (?? ).

The thesis is structured as follows: ?? introduces the reader to color centers and diamond as a host material. A discussion of SiV centers restricted to their most important luminous properties is presented. ?? familiarizes the reader with the essential experimental setup and methods deployed in this thesis to study SiV center luminescence. Various relevant methods of synthesizing sample nanodiamonds containing SiV centers are presented and discussed in ???. ?? is dedicated to the important topic of gauging the quality of fabricated samples. The results of charting the luminous properties of our nanodiamonds samples is presented in ???. Our attempts of coupling nanodiamonds hosting SiV centers to two different nano structures is investigated in ???. Finally we summarize and discuss the findings of this thesis in ??.

## **1.1 Coupling Nanodiamonds to Double Bowtie Antenna Structures**

Plasmonic nano-antennas are very recent devices designed to efficiently convert freely propagating optical radiation into localized energy and vice versa [?, ?, ?, ?, ?, ?]. Leveraging this unique property, integrating SiV centers with optical antennas creates coupled systems with a range of desirable features. These include enhanced photoluminescence emission and the ability to tailor photoluminescence spectra of the integrated emitters. The latter can be achieved by tuning the physical design parameters of the system including antenna geometry and emitter placement.

In this chapter we report on our efforts aimed at enhancing the properties of SiV centers by coupling them to optical double bowtie antennas. To this end we transfer selected nanodiamonds containing SiV centers to the target antenna structure using pick-and-place methods. After successful coupling we investigate the integrated structure experimentally. In addition to that we successfully relate some of our results to theoretical predictions.

In the following we give a short discussion of the most important properties of optical antennas. Then we sketch the actual coupling process and report on the optical properties of the resulting integrated structure. To our knowledge, our experiments were the first attempts of coupling SiV centers to plasmonic bowtie antennas.

### **1.1.1 Plasmonic Antennas**

Optical nano-antennas act as converters between propagating and localized electromagnetic fields. Thus, they can be used efficiently to couple photons in and out of

## 1.1. COUPLING NANODIAMONDS TO OPTICAL ANTENNAS. SIV CENTERS

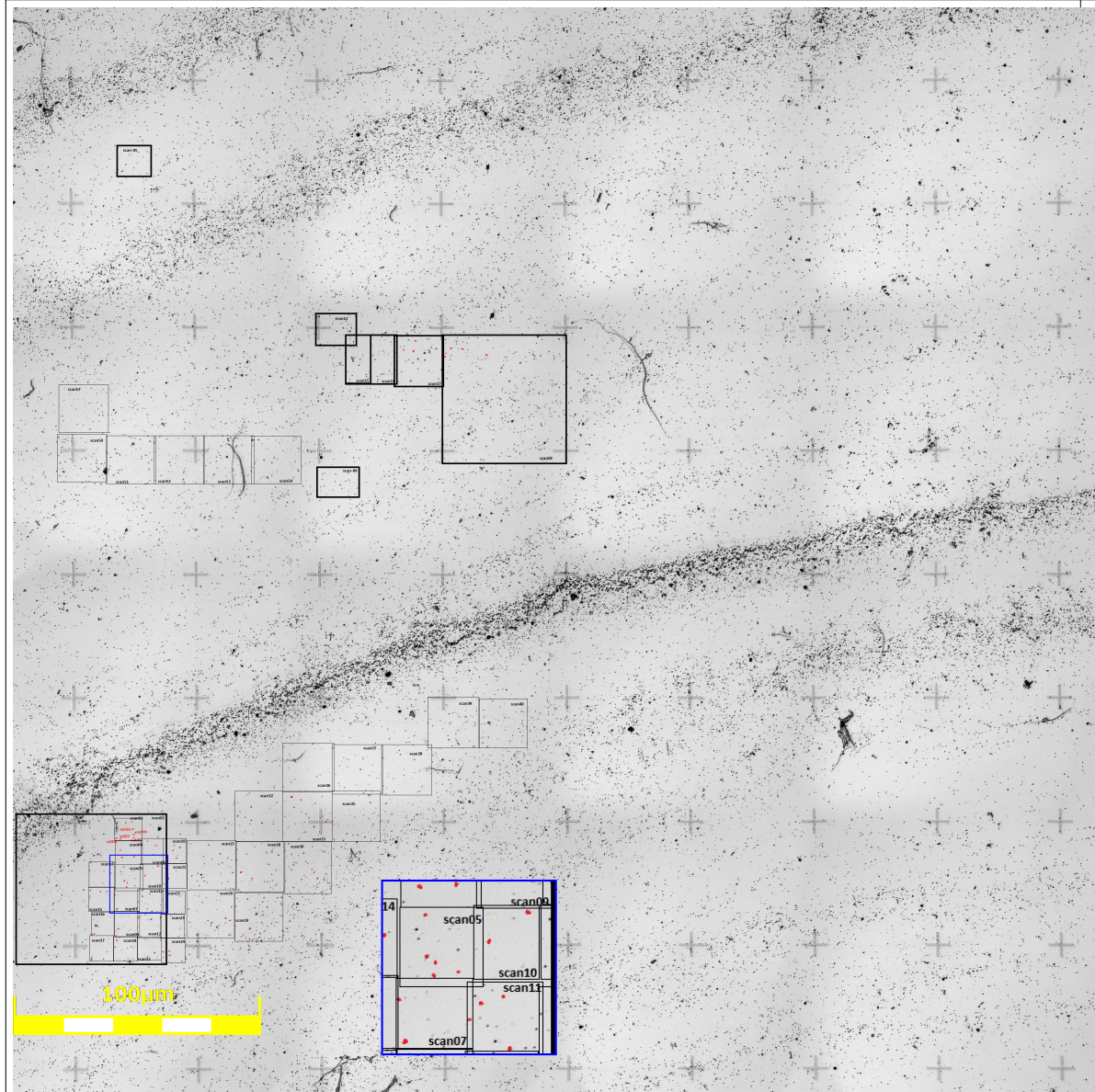


Figure 1.1: Sample surface of a  $0.5 \text{ mm} \times 0.5 \text{ mm}$  area of one of the investigated samples in search for suitable nanodiamonds. Black frames correspond to areas of which confocal scans were recorded to identify nanodiamonds emitting fluorescence light. Red colored dots indicate nanodiamonds which are isolated enough for the pick-and-place process and of which at least a photoluminescence spectrum and a saturation measurement and in some cases a  $g^{(2)}$  measurement were recorded. The inset shows a magnification of the area framed in blue for better visibility of the red colored dots.

nano-scale objects [5]. Due to their small physical sizes, comparable or smaller than the wavelength of visible light, they are capable of focusing optical fields to sub-diffraction-limited volumes, offering the ability to manipulate electromagnetic fields at nano-scales [?, ?]. This property, dubbed sub-wavelength confinement, has successfully been exploited to enhance the excitation and emission of quantum emitters [?, ?, ?, ?] and to modify their spectra [?]. Resulting practical applications include near-field optical microscopy [?], surface enhanced spectroscopy [?, ?] and molecular sensing [?].

A nano-antenna is a nano-structure made from materials such as noble metals like gold or silver. These metals have in common that they are very susceptible to being polarized by electro-magnetic fields. When illuminated by the incident electromagnetic radiation causes electrons in the metal to behave as a plasma that tends to move with respect to the atomic lattice. As a result excess charge at the opposite surfaces of the material accumulates and the material becomes temporarily polarized until restoring forces equilibrate the charge distribution.

Thus incident light of a given frequency induces oscillations in the free electron gas density in the surface layers of the metal. At resonance these light-induced oscillations exhibit modes of standing waves. The quasi-particles associated with these modes are known as localized surface plasmons (LSPs). For an in-depth treatment of LSPs in the context of nano-antennas we refer the reader to [?] and references therein.

Here it suffices to say, that LSPs facilitate the deciding property of optical antennas: Converting electromagnetic energy from the far-field into localized energy in the near-field. This allows, in combination with the high collection-efficiencies of nano-antennas, to efficiently couple visible radiation with wavelengths of hundreds of nanometers, into small effective spatial volumes of only a few nanometer in diameter.

To create a controlled hot-spot several antenna designs are possible. In the context of this thesis we rely on double bowtie antennas available via a collaboration with N. Rahbany, group of C. Couteau, University of Technology of Troyes. ?? illustrates the typical bowtie antenna.

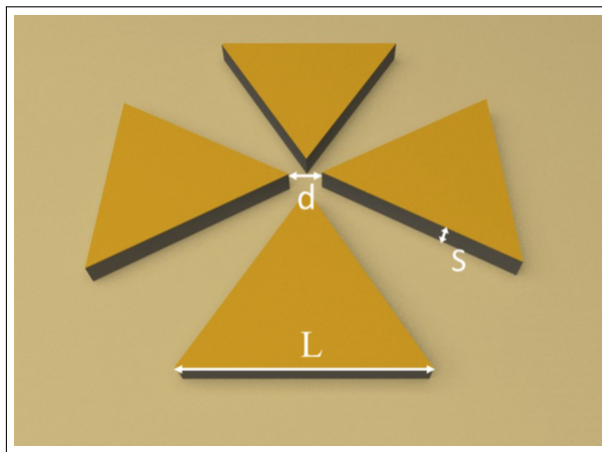


Figure 1.2: Schematic of a double bowtie antenna [?, 6, 7].

This antenna design utilizing a symmetric arrangement of four identical triangle-shaped blocks, separated by a small gap. This setup allows LSP modes local to individual blocks

to couple with each other resulting in the formation of an intense hot-spot in the center area [?], see ?? . The actual electromagnetic response of a double bowtie nano-antenna depends on its physical design parameters such as gap size, material used, geometry and size. Furthermore, properties of incident light such as wavelength and polarization determine antenna operation.

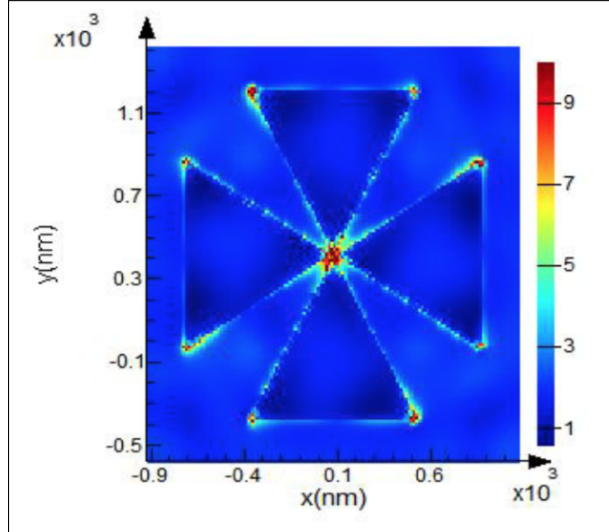


Figure 1.3: Simulation result of the electric field map of a gold double bowtie nano-antenna [?, 6, 7]. The structure has gap of  $d = 150 \text{ nm}$ , a side length of  $L = 2 \mu\text{m}$  and a thickness of  $S = 60 \text{ nm}$ . The center of the antenna exhibits an area of pronounced focus, the so-called hot-spot.

The improved electromagnetic field at the center of a metallic nano-antenna can be used to increase the spontaneous emission rate of emitters emitting at frequencies close to the resonance frequency of the antenna. This result is the known as Purcell effect [?]. The gap between the antenna arms acts as a resonant cavity providing a strong near field interaction with the emitter. This interaction modifies the density of states of the system, effectively providing additional modes for the emitter to decay into, thus amplifying its total decay rate. The amplification affects both radiative and non-radiative decay. The magnitude of the amplification for an emitter is quantified by the ratio of its enhanced decay rate to its free space decay rate, known as the Purcell factor  $F_p$ . This factor is proportional to  $Q/V_{eff}$  where  $Q$  denotes the quality of the antenna and  $V_{eff}$  the volume of the hot-spot. Thus antenna design must optimize  $F_p$  as a necessary condition for significant enhancement of fluorescence light emission.

In addition to the antennas local field enhancement, the emitters original quantum yield  $\eta_0$  influences the overall effectiveness of the emission enhancement. From theoretical considerations [?, ?, ?, ?], the modified quantum efficiency  $\eta$  of the combined system consisting of emitter and antenna can be obtained as

$$\eta = \frac{\eta_0}{\frac{1-\eta_0}{F_p} + \frac{\eta_0}{\eta_{ant}}}, \quad (1.3)$$

where  $\eta_{ant}$  denotes the fraction of fluorescence light which is not dissipated through losses in the metal of the antenna. It is clear that an emitter with  $\eta_0 \rightarrow 1$  will not profit from the Purcell effect. On the contrary, for realistic antennas with  $\eta_{ant} < 1$  antenna-induced losses reduce the overall quantum yield  $\eta$ . Consequently poor emitters with low initial  $\eta_0$  stand to profit the most from antenna-emitter coupling provided antennas are engineered well, i.e. they maximize their Purcell Factors and minimize their losses. For an in-depth review of plasmonic nano-antennas we refer the reader to [?] and references therein.

The presented considerations illustrate that due to their relatively low quantum efficiency, SiV centers are excellent candidates for coupling with antennas. Thus it is promising to exploit the improved electromagnetic field at the center of a double bowtie antenna to enhance the spontaneous emission rate of SiV centers and thus improve their merit as single photon sources.

### 1.1.2 Plasmonic Antenna Design and Simulation

To couple SiV centers to optical antennas, we work with gold double bowtie antennas on a gold substrate. In comparison with triangular, or single bowtie antennas, double bowtie antennas offer significantly improved intensity enhancements. Antennas were provided by N. Rahbany, group of C. Couteau, University of Technology of Troyes in a joined effort to explore the possibilities of combining antennas with SiV centers. The antennas themselves were fabricated using electron beam lithography, a technique suitable to imprint predetermined patterns onto a suitable substrate with nano-scale resolution [?]. ?? shows a SEM image of an array of antenna structures of various sizes. In ?? a detail of an individual double bowtie antenna is shown. It can be seen that the double bowtie antenna is placed in the center of another structure, a so-called bulls-eye antenna, consisting of multiple concentric gratings. When illuminated by a laser at a proper angle, the gratings excite surface plasmon polaritons (SPPs) which are directed towards the center of the structure. If a double bowtie antenna is present in the center, SPPs can interact with the LSPs of the double bow tie, leading to an even stronger localization of electromagnetic fields in the gap of the bowtie. While this interaction certainly merits exploration in the context of enhancing SiV centers, we omit the excitation of SPPs in our first exploration of the coupling of SiV centers and antennas. Thus the presence of the gratings can be ignored for our purposes. The reader interested in the details of bulls-eye antennas and their properties is referred to [?].

To effectively enhance the emission of an emitter by coupling it to an optical antenna, the emission wavelength must match the resonant wavelength of the antenna. In the context of SiV centers a value of 738 nm is required. Since this value can be considered constant, the design parameters of the antenna must be chosen such, that the resulting resonance matches it. An additional constraint is placed on the size of the antenna gap, since it must be big enough to accommodate nanodiamonds hosting SiV centers, the former are around 100 nm in size. However, it cannot be chosen arbitrarily big, since

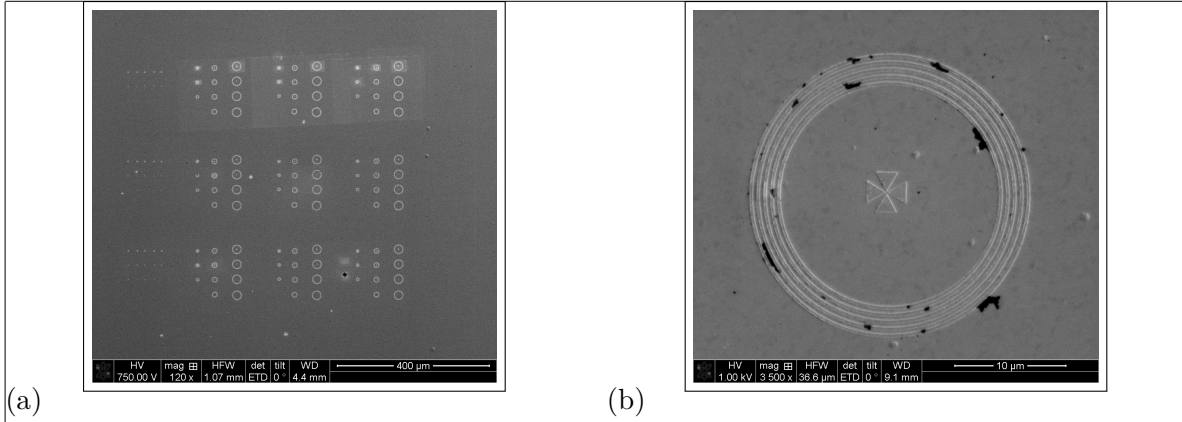


Figure 1.4: SEM images of antenna structures. (a) Overview of a field of antenna structures exhibiting various dimensions. (b) Detail of one antenna structure. In the middle the double bowtie design is visible. A grating structure consisting of multiple gratings is surrounding it.

bigger gaps lead to larger effective volumes and thus smaller Purcell Factors.

Using finite time difference domain (FDTD) simulation deploying Lumerical Software the design space of gold double bowtie nano-antennas on a gold substrate was explored [?]. Although we initially attempted to simulate antennas without a nanodiamond present in the gap, it was subsequently discovered that its ab initio inclusion yielded superior results. Thus to determine usable design parameters for our purposes, an integrated system combining antenna and nanodiamond was used. To better mimic experimental conditions and associated imperfections, the nanodiamond was placed slightly off-center in the gap.

In a series of simulation it was established that a gap-size of  $d = 150 \text{ nm}$ , a side length of  $L = 2 \mu\text{m}$  and a structure thickness of  $S = 60 \text{ nm}$  are feasible parameters as referred to in ???. The simulation required the index of refraction for gold which was taken from Palik [?, ?, ?, ?].

The resulting geometry hosting a nanodiamond is capable of producing a suitable hot-spot when excited.

Finally, to pin-point the resonant wavelength for the antenna hosting a nanodiamond, the electric field intensity is simulated as a function of the wavelength of the incident light. The resulting spectrum is shown in ???. Two resonant peaks are found. The intense major peak at 739 nm coincides exceptionally well with the SiV center emission wavelength 738 nm indicating successful antenna design. In addition to the major peak, an additional minor mode at a lower wavelength of 710 nm is found [7]. We remark that if the nanodiamond in the gap of the antenna is removed from the simulations, the minor feature vanishes. Thus the additional peak is well-attributed to the presence of the nanodiamond.

In summary, the combined simulation results suggest, that the engineered system of nano-antenna and nanodiamond is well suited to effectively enhance the emission from an SiV center hosted in the nanodiamond. In the following sections we report on the

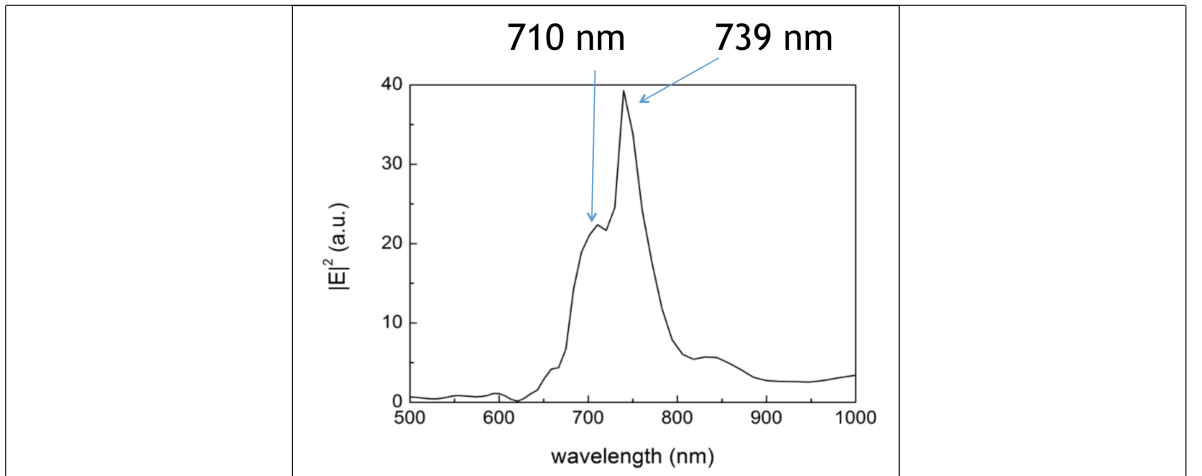


Figure 1.5: FDTD simulation of the electric field intensity of a double bowtie nano-antenna as a function of the wavelength of incident light. Two peaks are identified. The major peak corresponds exceptionally well with SiV center emission at 738 nm. The minor peak is attributed to the presence of a nanodiamond.

experimental realization of this preposition.

### 1.1.3 SiV center in a Plasmonic Double Bowtie Antenna

In the following we report on our attempts to couple SiV centers to gold double bowtie nano-antennas in order to study the properties of the resulting integrated system. Ideally, a suitable nanodiamond containing exactly one SiV center is placed in the center of the antenna. The term suitable is used to summarize both desirable spectroscopic properties such as narrow-bandwidth saturated single-photon emission as well as technical requirements such as nanodiamond size and degree of isolation on the surface. Naturally, the odds of identifying and addressing a nanodiamond fulfilling all these criteria simultaneously are small. As a result identifying a perfect candidate for coupling is prohibitively time-consuming. ?? shows a  $0.5 \text{ mm} \times 0.5 \text{ mm}$  area of the surface of one of the samples which was used to identify suitable nanodiamonds. The black dots are nanodiamonds. It can be seen, that the concentration of the nanodiamonds and therefore the isolation of nanodiamonds varies. The black frames correspond to areas of which confocal scans were recorded to identify nanodiamonds emitting fluorescence light. The red dots indicate nanodiamonds which are isolated and large enough for the pick-and-place process and of which at least a photoluminescence spectrum and a saturation measurement and in some cases a  $g^{(2)}$  measurement were recorded. Only two of the measurements performed on this sample revealed a favorable spectrum, emission saturation and at least a small dip in the  $g^{(2)}$  function indicating a small amount of SiV centers.

To mitigate this difficulty we decided to relax the condition of exactly one SiV center per nanodiamond and initiate our exploratory work with nanodiamonds containing several,

## 1.1. COUPLING NANODIAMONDS TO OPTICAL ANTENNAS. SIV CENTERS

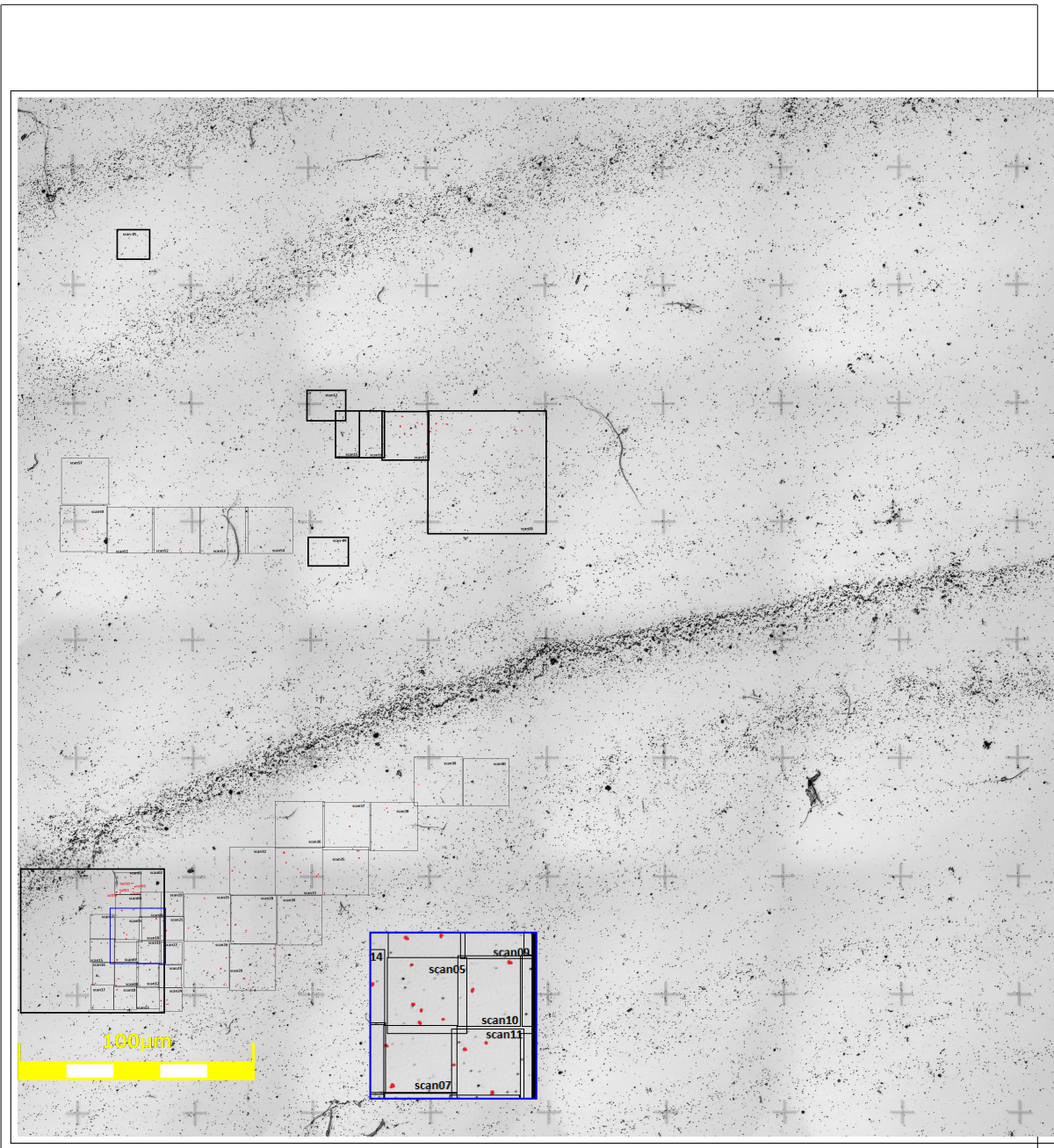


Figure 1.6: Laser scanning microscope scan of one of a  $0.5\text{ mm} \times 0.5\text{ mm}$  area of the investigated samples in search for suitable nanodiamonds. Black frames correspond to areas of which confocal scans were recorded to identify nanodiamonds emitting fluorescence light. Red colored dots indicate nanodiamonds which are isolated enough for the pick-and-place process and of which at least a photoluminescence spectrum and a saturation measurement and in some cases a  $g^{(2)}$  measurement were recorded. The inset shows a magnification of the area framed in blue for better visibility of the red colored dots.

potentially many active SiV centers. Relying on  $g^{(2)}$  measurements we identify two interesting classes of nanodiamonds. The first class consists of nanodiamonds containing large ensembles of SiV centers acting as coherent emitters. The fluorescence light received from large ensemble of emitters is mainly coherent, leading to a flat response in the  $g^{(2)}(0)$  function. The second class of nanodiamonds we investigate features nanodiamonds hosting multiple SiV centers. As a result relevant  $g^{(2)}(0)$  measurements report weak but discernible anti-bunching dips. Both classes have in common that relevant nanodiamond specimen are significantly easier to obtain than nanodiamonds containing singleton SiV centers. Thus nanodiamonds containing ensembles of SiV centers as well as nanodiamonds containing few SiV centers are both valid starting points for our work. It is likely that the experience gained during our preliminary explorations will be valuable once nanodiamonds containing singleton SiV centers become available. In the following sections we report on our efforts to couple nanodiamonds containing SiV centers to antennas. We illustrate the coupling process and its challenges and discuss relevant results regarding the coupling of nanodiamonds of the classes described above. We close the chapter with a short discussion and suggestions for further research.

## Nanodiamonds Containing Ensembles of SiV centers Coupled to Antennas

### Remark:

fuer ?? braucht noch das richtige bild. also eine g2 function mit coherent light

The nanodiamonds used for the approach of coupling ensembles of SiV centers to an antenna were wet-milled from a CVD diamond film<sup>1</sup>. The solution of nanodiamonds exhibiting a median size of 100 nm was spin-coated on an iridium substrate treated with Piranha etch (sample of type insitu100). To ensure that a preselected nanodiamond exhibiting preferred optical properties can reliably be located, the iridium substrate was engraved with reference cross markers produced by a focused ion beam after the spin-coating process. After spin-coating, the sample was placed in an oven for 3 h at 450 °C to oxidize the surface and remove any residual graphite and amorphous carbon. See ?? for more information.

To determine the position of nanodiamonds on the original substrate, first a scan with a commercial laser scanning microscope (LSM) was performed as described in ???. ?? shows a part of an obtained LSM image. After transferring the sample into the confocal setup, confocal fluorescence light scans of the corresponding areas are performed to identify nanodiamonds containing active emitters. The scanned area is shown in ???. It corresponds to the area shaded blue in ???. Thus, upon close inspection some of the bright spots appearing in the fluorescence light scan can be associated with selected nanodiamonds in ?? by eye. The correspondence between the SEM and LSM images in conjunction with the cross-markers on the substrates allows to precisely locate preselected nanodiamonds containing suitable emitter in the SEM.

---

<sup>1</sup>wet-milling performed by A. Muzha, group of A. Krueger, Julius-Maximilians Universität Würzburg, diamond film grown by group of O. Williams, School of Engineering, Cardiff University

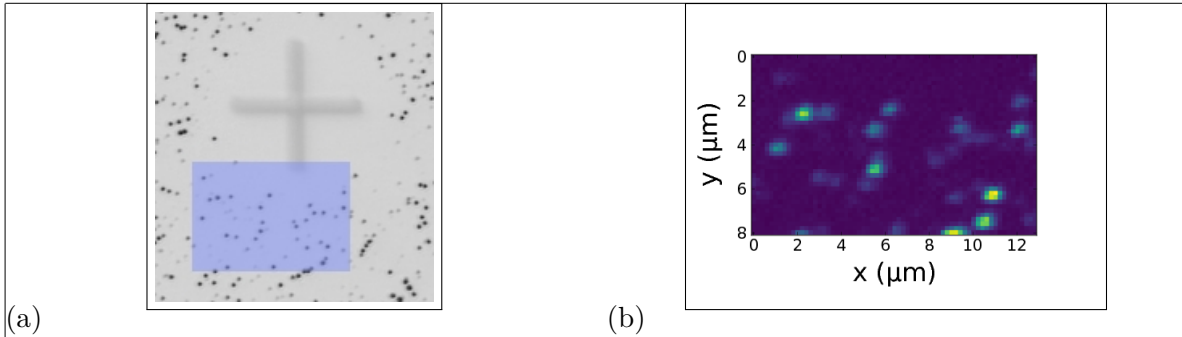


Figure 1.7: (a) Picture recorded with a commercial high resolution laser scanning microscope. Black dots are individual nanodiamonds. The cross-marker serves as an orientation aid. The area shaded in blue represents the photoluminescence scan in image (b). (b) Photoluminescence scan of a  $8 \mu\text{m} \times 13 \mu\text{m}$ .

The most promising candidate nanodiamonds are characterized by fluorescence light spectra with very narrow zero-phonon-lines and minimal phonon side band features. ?? shows the spectrum stemming from one such preselected nanodiamond. The ZPL feature exhibits a center wavelength of  $(738.55 \pm 0.01)$  nm and a linewidth of  $(5.00 \pm 0.03)$  nm, corresponding well with the ZPL of unstrained SiV centers. Photon autocorrelation measurements revealed that the nanodiamond contains an ensemble of SiV centers collectively generating coherent fluorescence light light, see ?? .

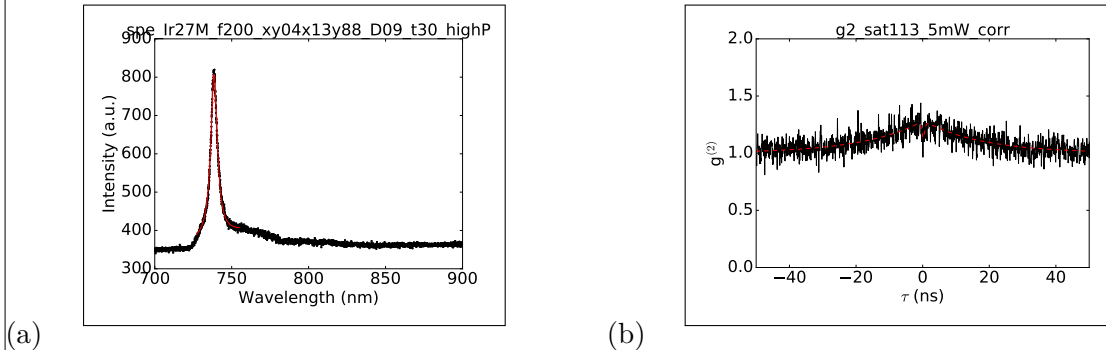


Figure 1.8: a) PL spectrum of the emitter in the preselected nanodiamond at room temperature. Black: experimental results; red: fit to experimental data, which yields a ZPL center wavelength of  $(738.55 \pm 0.01)$  nm and a linewidth of  $(5.00 \pm 0.03)$  nm. b) Intensity autocorrelation function recorded for the ensemble of emitters hosted by the nanodiamond. The flat response indicates the coherent nature of the fluorescence light light.

After a proper candidate for coupling with an antenna has been identified, it needs to be relocated from its original substrate to the antenna. To this end a pick-and-place process introduced in ?? is used. A complete illustration of the steps involved is given in ?? .

The gold surface of the plasmonic antenna exhibited strong adhesion forces between

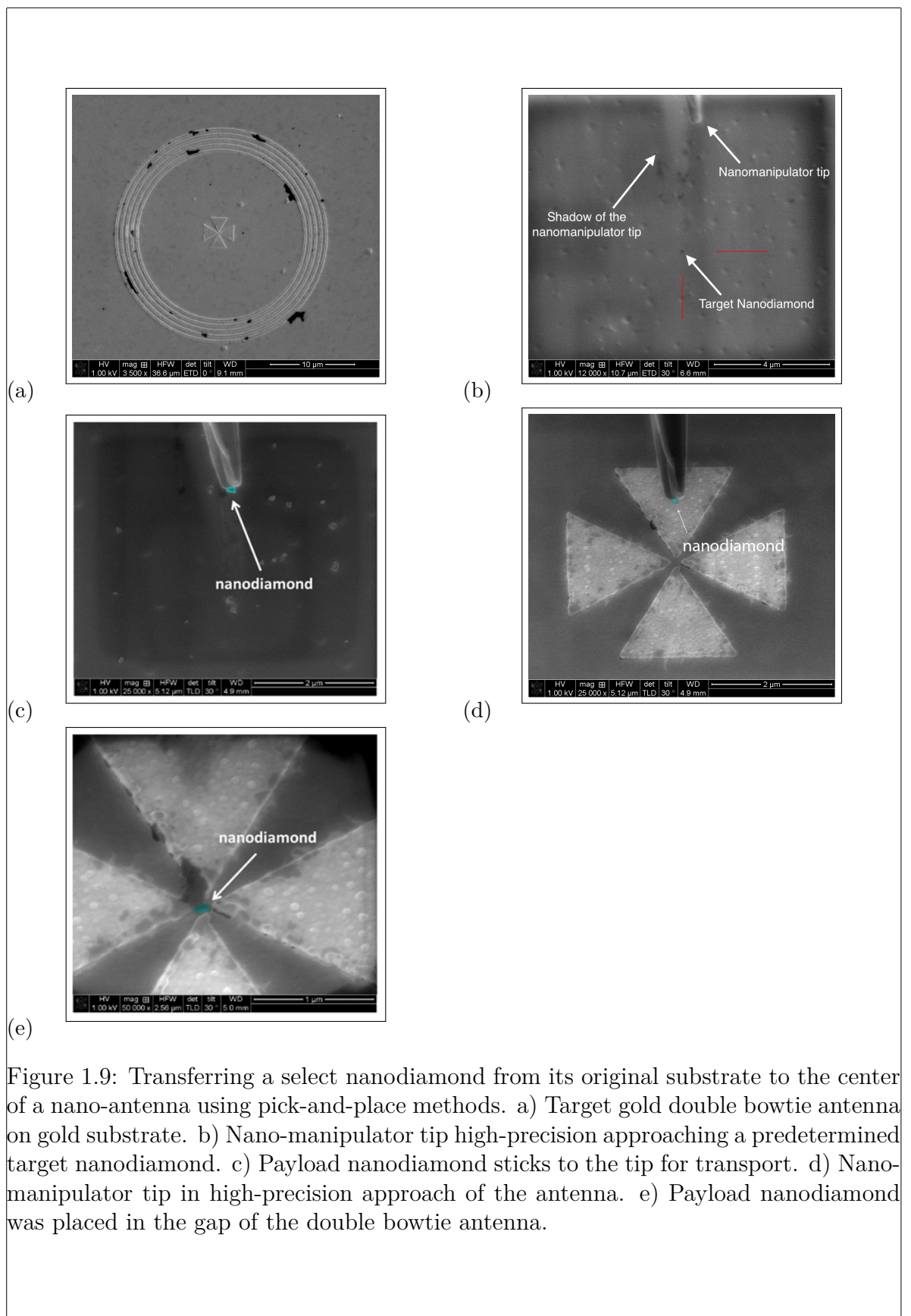


Figure 1.9: Transferring a select nanodiamond from its original substrate to the center of a nano-antenna using pick-and-place methods. a) Target gold double bowtie antenna on gold substrate. b) Nano-manipulator tip high-precision approaching a predetermined target nanodiamond. c) Payload nanodiamond sticks to the tip for transport. d) Nano-manipulator tip in high-precision approach of the antenna. e) Payload nanodiamond was placed in the gap of the double bowtie antenna.

the antenna surface and the nanodiamond. Once the nanodiamond touched the gold, it could not be picked up again with the tungsten tip. The nanodiamond first touched the antenna structure a few nanometers away from the gap and immediately stucked to the surface, on top of one of the triangles. Therefore, the nanodiamond had to be pushed into the gap with the nano-manipulator tip. This process caused some damage to the antenna structure. The damage is visible as black area at the tip of the top triangle in ?? . Luckily, FDTD simulations of damaged antennas reveal that this modification of the antenna hardly influences the antenna resonance.

After successful placement, the antenna sample is installed in the confocal setup. The antenna itself was located during a scan of the sample surface under white light illumination. A scan of the antenna is performed in the confocal setup using a 660 nm continuous wave laser. It serves to locate the middle of the antenna structure and therefore the nanodiamond which had been placed there. An outline of the rings is visible in an overview scan of the antenna structure shown in ?? . Zooming in to the exact center of the rings, some of the edges of the bowtie antenna are vaguely visible in ?? .

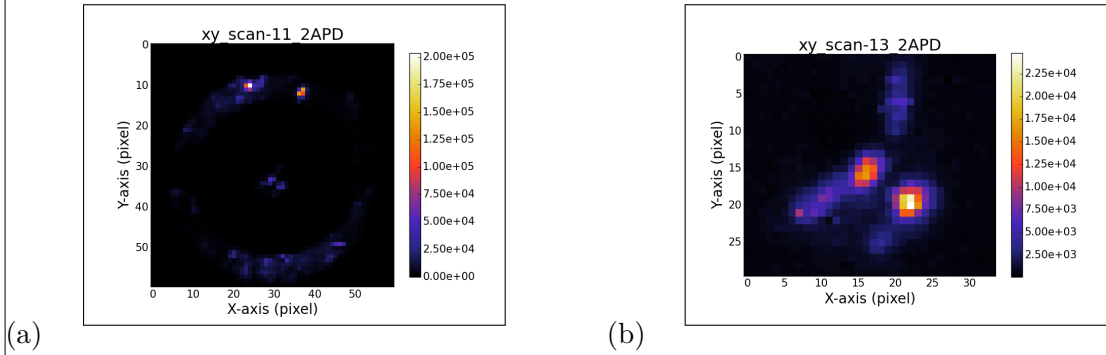


Figure 1.10: (a) Confocal scan of the double bowtie antenna where a nanodiamond containing multiple SiV centers had been placed. The rings are visible. (b) Detail scan of the triangles of the same antenna structure, which make up the double bowtie antenna. While the separate triangle cannot be seen, some edges and two bright spots are visible. To identify the place of the nanodiamond we compare the middle point of the rings in (a), the point of intersection of the edges and the bright spot and conclude that the upper bright spot in (b) is the location of the nanodiamond.

These images suffices to locate the nanodiamond with sufficient precision to measure PL spectra. The PL spectrum of the ensemble of SiV centers in the nanodiamond is shown in ?? . It can be seen that at 738 nm a major peak is present, almost exactly at the same wavelength than the SiV center zero-phonon-line, i.e. 739 nm. The additional minor peak at 726 nm is attributed to the antenna resonance mode. We remark that, any damage sustained through electron radiation during the pick-and-place process is likely not sufficient to invalidate the nanodiamond. This is expected as a large ensemble of SiV centers can easily lose several emitters without any noticeable difference in the optical properties. Needless to say, the exact opposite is true for nanodiamonds with very few hosted SiV centers making them risky to work with.

We verified successful coupling of the ensemble of SiV centers to the antenna by combining experimental and numerical results. In particular, we convolve the experimental PL spectrum of the nanodiamond measured before placing it in the nano-antenna, see ?? , with the intensity spectrum of the nano-antenna obtained by means of simulations given in ?? . The result of the convolution is the spectrum given in ?? . The agreement with the measured spectrum in ?? is almost perfect, indicating successful coupling of emitters and antenna. At the same time we confirm that the minor peak in ?? is indeed due to the antenna resonance.

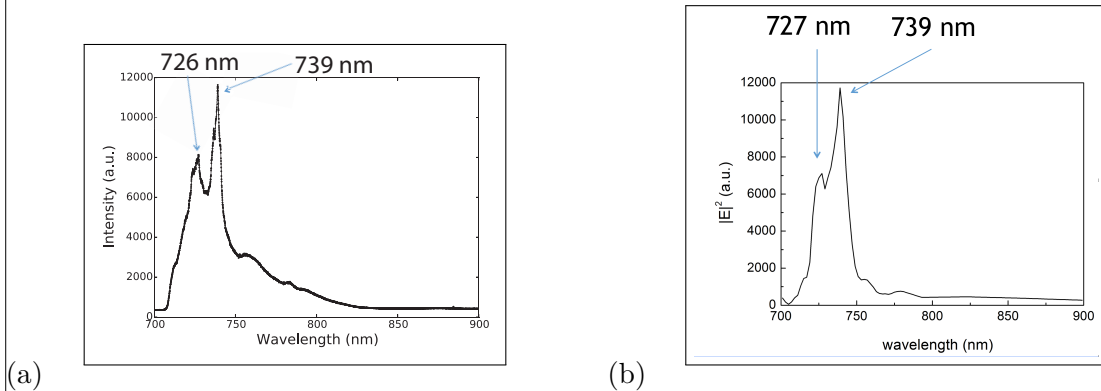


Figure 1.11: (a) Measured PL spectrum of the emitter after placing the nanodiamond into the nano-antenna, (b) Convolution of the spectrum of the measured PL spectrum of the emitter before pick-and-place, see ?? , and the simulated resonance spectrum of the nano-antenna, see ?? .

Finally, keeping experimental conditions unchanged, we measure a spectrum of an identical antenna without a nanodiamond present in order to rule out surprising artifacts induced by the antenna itself. The resulting spectrum is given in ?? .

At this point one must resist the temptation of comparing the values of the intensity maxima of the spectra in ?? and ?? in order to determine the enhancement the ensemble of emitters experiences. These values inherently do not allow a meaningful comparison.

A meaningful comparison can in principle be achieved via intensity saturation measurements. By measuring the saturation intensities before and after insertion into the antenna and accounting for effects related to the polarization of emitters, the magnitude of the Purcell enhancement can be determined. Unfortunately, these methods are reserved for single emitters and do not apply for ensembles of SiV centers. Thus at this point we have no method to determine the Purcell enhancement ensembles of SiV centers experience.

In summary, in this section we showed that coupling of nanodiamonds containing ensembles of SiV centers with gold double bowtie antennas is feasible using a pick-and-place approach. Furthermore we verified that the coupling is indeed present after the nanodiamond was placed in the gap of the antenna. Unfortunately, at present there is no reliable method available to us to quantify the magnitude of fluorescence light enhancement experienced by the SiV center ensemble.

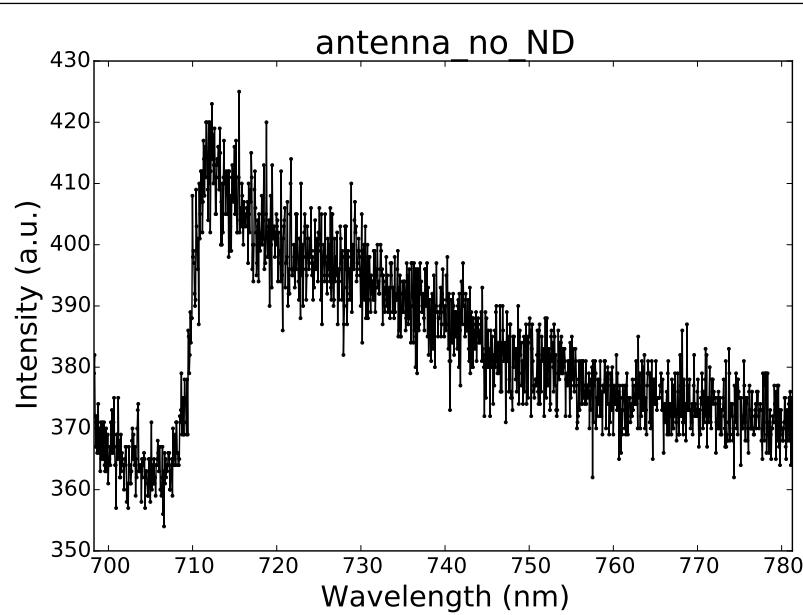


Figure 1.12: Spectrum of a gold double bowtie nano-antenna without a nanodiamond present.

### Nanodiamonds Containing Few SiV centers Coupled to Antennas

#### Remark:

- FDTD bilder fehlen komplett. Muessen unten eingefuegt werden.
- FDTD simulation fuer verschiedenen dipole orientations werden kurz erwaeahnt, gibts da bilder?
- Fuer das spectrum von nanodiamond + antenne sind die locations von den subpeaks wichtig? Irgendwo sollte erwaeahnt werden, dass der neue major peak nicht dort ist wo man die SiV center zero-phonon-line erwarten wuerde.
- Die fits an die subpeaks von dem spectrum nanodiamond + antenne werden nicht erklaert. Wenn die nicht wichtig sind, sollte man sie zumindest beilaeufig erwaeahn.

After a first successful validation of inserting nanodiamonds hosting large ensembles of SiV centers into a gold double bowtie antenna, we attempt to select nanodiamonds containing a comparatively small number of SiV centers. Suitable nanodiamonds show an anti-bunching dip in the  $g^{(2)}$  function in addition to count-rate saturation. This can be regarded an intermediate step towards using nanodiamonds containing singleton SiV centers. We stress that in comparison to nanodiamonds hosting large ensembles of emitters, nanodiamonds containing only a few emitters are already difficult to identify. Naturally, technical requirements applying to candidate nanodiamonds such as sufficiently isolation for picking it up in the pick-and-place process and a size not larger than that of the antenna gap still need to be observed.

The starting material for the nanodiamonds used here was an electronic grade diamond film produced by the company rho-BeSt coating (now renamed to CarbonCompetence). The film was then milled in a bead-assisted sonic disintegration process<sup>2</sup> to nanodiamonds of a median size of approximately 100 nm. The nanodiamonds were drop-cast at 60 °C onto an iridium substrate containing cross markers. Prior to drop-casting the substrate was cleaned with Piranha etch.

Given samples containing nanodiamonds the tedious task of identifying potential candidates for transfer to the antenna. As described in the previous section, a commercial laser scanning microscope (LSM) is used to identify nanodiamonds on the substrate. Using the cross markers to address their exact positions, a corresponding fluorescence light scan allow us to single out nanodiamonds with bright emission. We further test the suitability of potential candidates as follows. First, a saturation curve is recorded to establish whether the SiV centers in a nanodiamond saturate. Since saturation is a necessary albeit not sufficient condition for single-photon emission, only nanodiamonds that saturate are capable of showing an anti-bunching dip in the  $g^{(2)}$  function. Note that, measuring the  $g^{(2)}$  function potentially requires hour-long measurements, while determining saturation requires merely seconds. Thus, in search of candidate nanodiamonds we may use the saturation behavior as a quick check whether a candidate is feasible to follow up with a lengthy  $g^{(2)}$  function measurement. For nanodiamonds containing SiV centers showing saturation we then check the spectrum to assert that the emitters are indeed SiV centers. After this last check  $g^{(2)}$  function measurements are established.

After a significant search, involving a sizable number of discarded candidates, a nanodiamond with a discernible anti-bunching dip was found. ?? shows its  $g^{(2)}$  function function while ?? reports its saturation curve. While the dip in  $g^{(2)}$  function is quite weak, it is present and a fitting it was possible. This indicates that the nanodiamond neither contains a singleton SiV center nor does it host enough SiV centers to emit coherent light. Thus we conclude that a limited number of SiV centers must be present. While it is not possible to quantify the number of emitters directly, the candidate sufficiently differs from nanodiamonds hosting large ensembles of SiV centers. Thus it is viable to take it to the stage of coupling.

In order to relocate the identified nanodiamond to the center of a gold double bowtie antenna we repeat the pick-and-place procedure described in the previous section, see ?? . We remark at this point that since the nanodiamond in question contains fewer SiV centers as compared to the nanodiamonds hosting large ensembles of SiV centers, it is expected to be less resilient to adverse effects such as the electron radiation present during the pick-and-place process.

After a successful relocation, the sample containing the antenna is mounted in the confocal setup to investigate the properties of the combined system consisting of antenna and SiV centers. ?? gives the spectrum of the candidate nanodiamond after being relocated to the center of a gold double bowtie antenna. Interestingly we find a multitude of individual peaks in the vicinity of the SiV center zero-phonon-line line. In addition we find that the sideband appears more pronounced in relation to the intensity of the ma-

---

<sup>2</sup>A. Krueger, Julius-Maximilians Universität Würzburg

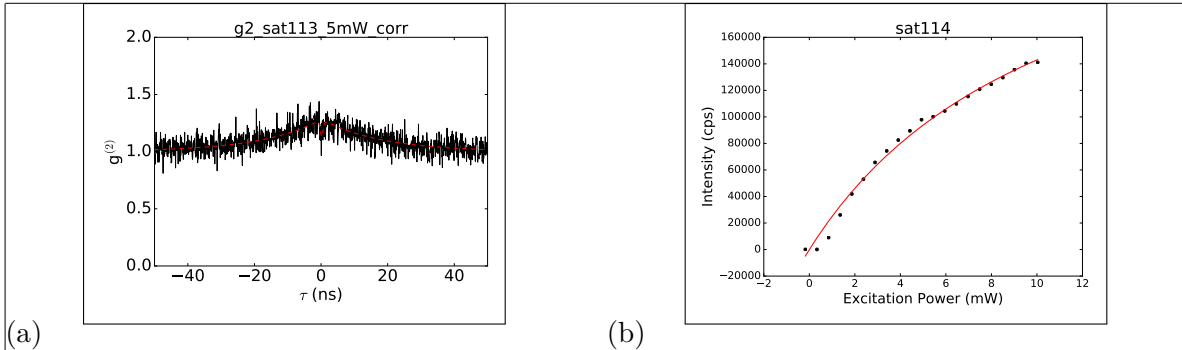


Figure 1.13: (a) The  $g^{(2)}$  function of the preselected nanodiamond believed to host a limited number of SiV centers. A dip at  $g^{(2)}(0)$  is present, however its decrease is not sufficient for a singleton SiV center. This indicates that a limited number of SiV centers is present since the absence of a dip can only be measured under coherent emission, i.e. for larger ensembles of SiV centers. The dashed red line gives a fit to the data.

cps zu a.u. aendern

. (b) Saturation curve of the same emitter

zahlen fuer sat eintragen

. Data points are black, fitted curve red.

major feature after the nanodiamond has been relocated to the antenna. Due to the shape of the recorded sideband we conjecture that it arises as a combination of the phonon side bands associated with individual SiV centers and additional contributions due to fluorescent contaminations. ?? showing the spectrum of the same nanodiamond before being relocated to the antenna. Here the phonon side band is weaker in comparison to the zero-phonon-line feature.

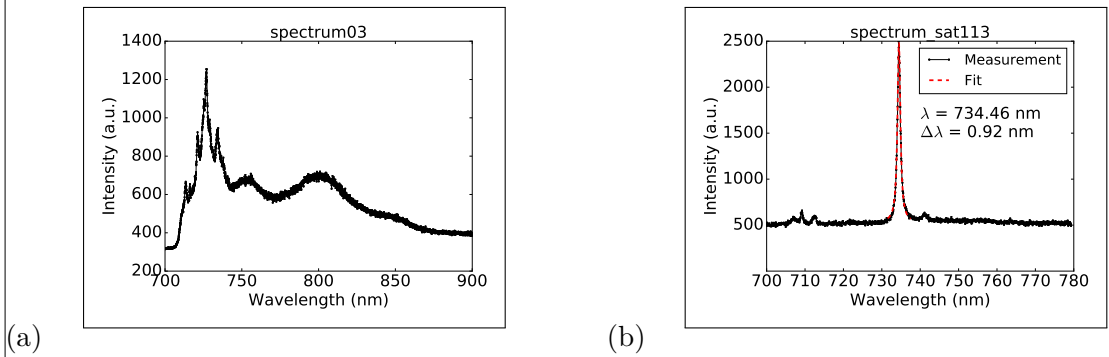


Figure 1.14: (a) Spectrum of the preselected nanodiamond hosting few SiV centers after being relocated to the center of a double bowtie antenna. (b) Spectrum of the same nanodiamond before relocation.

To exclude the possibility that the obtained peaks are artifacts due to misalignment of the experimental setup, we rechecked the alignment which proved to be precise.

To reverify the obtained spectrum, we repeated the measurement. Unfortunately, we

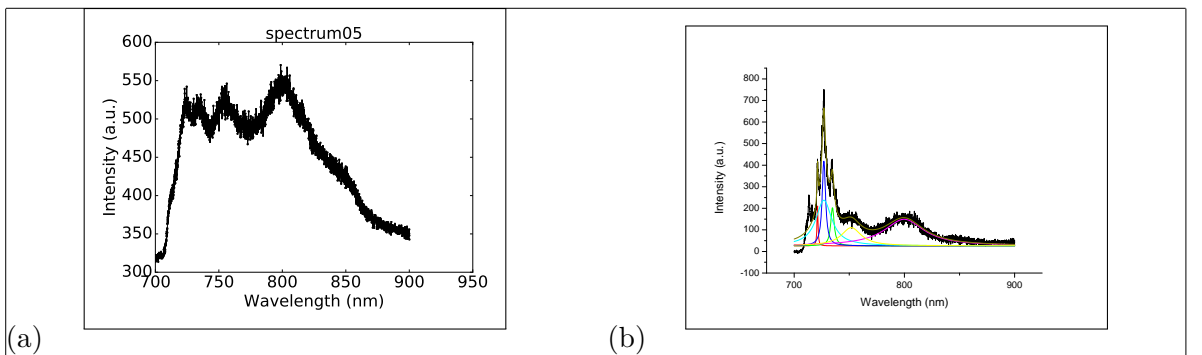


Figure 1.15: (a) Spectrum of the nanodiamond hosting few SiV centers coupled to the double bowtie antenna after the emitter bleached. (b) Background corrected spectrum of the transferred nanodiamond in the double bowtie antenna. Peaks are fitted, results of the fits are the colored lines. For background correction, the spectrum in (a) was used.

obtained an entirely different result, showing only a broad background seen in ?? . After checking in the confocal scan that the measurement was performed at the correct position, we had to conclude that all of the SiV centers hosted by the nanodiamond permanently bleached after recording the spectrum seen in ?? . It is likely that continued application of energy from the laser triggered this effect as earlier independent measurements established that SiV centers exhibit an increased likelihood of bleaching after being exposed to electron radiation []. Thus we conclude that the exposure to electron radiation during the pick-and-place left the SiV centers in an unstable state susceptible to bleaching.

Even though the nanodiamond was invalidated for further measurements, the spectrum that was obtained remains to be discussed further. To better understand the obtained observations, we turn to FDTD calculations of nanodiamond coupled to a gold plasmonic double bowtie antenna as described in the beginning of this chapter. In particular, we fold the spectrum of the nanodiamond before insertion into the antenna as given in ?? with the simulation spectrum of the integrated system consisting of nanodiamond and antenna. The simulation result thus constitutes a prediction of what we the spectrum in ?? should look like. ?? illustrates the simulation prediction and demonstrates that we have no reason to expect the to see the peaks between 700 nm to 750 nm observed experimentally. Hence we must conclude that the spectrum of the nanodiamond was modified during the pick-and-place process. While it is not possible to pinpoint exactly which circumstance caused the modification, several effects could influence the observed spectra.

First, the electron radiation itself. While it lacks the energy to modify the lattice itself, it can influence the electrons present and in particular may modify the charge state of SiV centers. As was mentioned before, electron radiation was linked to increased likelihood of photo-bleaching.

Next, during the pick-and-place process it is possible that the nanodiamond collects additional contaminating matter on its surface. Contaminations may be fluorescing

put in  
pictures  
for fdtd  
results  
and ref-  
erence  
them

## 1.1. COUPLING NANODIAMONDS TO OPTICAL ANTENNAS. SiV CENTERS

themselves, thus modifying the spectrum. The fact that we record a significant sideband signal in ?? supports this conjecture.

Yet another property of SiV centers which should not be neglected is their dipole orientation interacting with the antenna. Conducting dedicated FDTD simulations with a focus on different dipole orientations indicated a dramatic effect on the resulting spectra. Therefore, future experiments aiming to investigate the effect of coupling nanodiamonds containing few SiV centers to antennas should include polarization measurements to experimentally quantify the impact of the emitter orientation.

As it stands, the most likely explanation of the recorded spectrum consists of a combination of the discussed effects. Since the nanodiamond bleached almost immediately no further measurements were possible. It is thus advised to repeat the experiment hoping for a nanodiamond that manages to complete the pick-and-place process unharmed. At the moment it is not clear if this can be done, thus further investigation is required.

---

---

# Bibliography

- [1] J. Y. Cheung, C. J. Chunnillall, E. R. Woolliams, N. P. Fox, J. R. Mountford, J. Wang, and P. J. Thomas. The quantum candela: a re-definition of the standard units for optical radiation. *Journal of Modern Optics*, 54(2-3):373–396, jan 2007. 1, 2
- [2] Matthias Bock, Andreas Lenhard, Christopher Chunnillall, and Christoph Becher. Highly efficient heralded single-photon source for telecom wavelengths based on a PPLN waveguide. *Optics Express*, 24(21):23992, 2016. 3
- [3] Beatrice Rodiek, Marco Lopez, Helmuth Hofer, Geiland Porrovecchio, Marek Smid, Xiao-Liu Chu, Stephan Gotzinger, Vahid Sandoghdar, Sarah Lindner, Christoph Becher, and Stefan Kuck. Experimental realization of an absolute single-photon source based on a single nitrogen vacancy center in a nanodiamond. *Optica*, 4(1):71, 2017. 4
- [4] Aigar Vaigu, Geiland Porrovecchio, Xiao Liu Chu, Sarah Lindner, Marek Smid, Albert Manninen, Christoph Becher, Vahid Sandoghdar, Stephan Götzinger, and Erkki Ikonen. Experimental demonstration of a predictable single photon source with variable photon flux. *Metrologia*, 54(2):218–223, 2017. 4
- [5] Alberto G Curto, Giorgio Volpe, Tim H Taminiau, Mark P Kreuzer, Romain Quidant, and Niek F van Hulst. Unidirectional emission of a quantum dot coupled to a nanoantenna. *Science (New York, N.Y.)*, 329(5994):930–933, aug 2010. 7
- [6] N. Rahbany, W. Geng, S. Blaize, R. Salas-Montiel, R. Bachelot, and C. Couteau. Integrated plasmonic double bowtie / ring grating structure for enhanced electric field confinement. *Nanospectroscopy*, 1(1):61–66, 2015. 7, 8
- [7] Nancy Rahbany. Towards integrated optics at the nanoscale : plasmon-emitter coupling using plasmonic structures. 2016. 7, 8, 10